GLOBAL BIOGEOCHEMICAL CYCLES, VOL. 16, NO. 0, XXXX, doi:10.1029/2001GB001838, 2002

An integrated model of soil, hydrology, and vegetation for carbon dynamics in wetland ecosystems

Yu Zhang[1] and Changsheng Li

Complex Systems Research Center, Institute for the Study of Earth, Ocean and Space, University of New Hampshire, Durham, New Hampshire, USA

Carl C. Trettin and Harbin Li

Center for Forested Wetlands Research, USDA Forest Service, Charleston, South Carolina, USA

Ge Sun

Southern Global Change Program, North Carolina State University, Raleigh, North Carolina, USA

Received 26 November 2001; revised 10 May 2002; accepted 16 May 2002; published XX Month 2002.

[1] Wetland ecosystems are an important component in global carbon (C) cycles and may exert a large influence on global climate change. Predictions of C dynamics require us to consider interactions among many critical factors of soil, hydrology, and vegetation. However, few such integrated C models exist for wetland ecosystems. We developed a simulation model, Wetland-DNDC, for C dynamics including methane (CH_4) emissions in wetland ecosystems. The general structure of the model was adopted from PnET-N-DNDC, a process-oriented biogeochemical model that simulates C and N dynamics in upland forest ecosystems. We developed new functions and algorithms to capture the unique features of C dynamics under wetland conditions. Major modifications were made which focus on quantifying water table dynamics, soil thermal dynamics, growth of mosses and herbaceous plants, and soil biogeochemical processes under anaerobic conditions. In this paper, we report new developments made for Wetland-DNDC, as well as tests against observations from three wetland sites in Northern America. Validation results show that the model's predictions are in good agreement with measurements of water table dynamics, soil temperature, CH_4 fluxes, net ecosystem productivity (NEP), and annual C budgets. Sensitivity analysis indicates that the most critical input factors include temperature, water outflow parameters, initial soil C content, and plant photosynthesis capacity. NEP and CH_4 emissions are sensitive to many of the input variables required by different components of the model. These results suggest that integrated modeling with soil, hydrology, vegetation, and climate is essential to predict C cycles in wetland ecosystems. *INDEX TERMS:* 1615 Global Change: Biogeochemical processes (4805); 1890 Hydrology: Wetlands; *KEYWORDS:* wetland, model, carbon cycles, methane emissions, hydrology

Citation: Zhang, Y., C. Li, C. C. Trettin, H. Li, and G. Sun, An integrated model of soil, hydrology, and vegetation for carbon dynamics in wetland ecosystems, *Global Biogeochem. Cycles*, *16*(0), XXXX, doi:10.1029/2001GB001838, 2002.

1. Introduction

[2] Wetlands are an important component of the terrestrial landscapes that exert a great influence over global carbon (C) cycle and climate change. Wetlands contain 15–22% of the global terrestrial carbon [*Eswaran et al.*, 1995; *Gorham*, 1991] and contribute 15–20% of the global methane (CH_4) emissions to the atmosphere [*Aselmann and Crutzen*, 1989; *Matthews and Fung*, 1987]. Wetland ecosystems have unique characteristics affecting C dynamics. For example, the high water table and its fluctuation are the primary factors driving decomposition [*Moore and Dalva*, 1997; *DeBusk and Reddy*, 1988], plant C fixation [*Bubier*, 1995], CH_4 production and consumption [*Moore and Roulet*, 1993; *Bellisario et al.*, 1999], and other biogeochemical processes in the wetlands. Some researchers suggest that small changes in water table or temperature can perturb the C balance in the peatlands due to alterations in soil organic matter decomposition and/or plant production [*Bubier et al.*, 1998; *Silvola et al.*, 1996; *Shurpali et al.*, 1995]. Accordingly, quantifying the processes and controls on wetland C dynamics, including CH_4 emission, is required to assess impacts of climate change or management alternatives on wetland ecosystems.

[1]Now at Environmental Monitoring Section, Canada Center for Remote Sensing, Ottawa, Ontario, Canada.

0886-6236/02/2001GB001838$12.00

[3] Carbon cycles and CH_4 emission in wetland ecosystems are regulated by a series of interacting processes between soil, hydrology, and vegetation. For example, hydrological processes have a great impact on soil thermal dynamics; soil thermal and hydrological conditions influence plant growth and soil C dynamics (e.g., decomposition, CH_4 production, and oxidation); plant growth affects hydrological processes through evapotranspiration and interception; and soil, water, and plants work in conjunction to affect CH_4 production and transport. For handling these complex interactions, process-oriented models should be the most productive approach to synthesize our knowledge. There are few existing wetland models which are comprehensive enough to integrate most of the important processes for wetland ecosystems [*Mitsch et al.*, 1988] although many C models have been developed for upland ecosystems and used for global-scale C fluxes without explicitly identifying wetland ecosystems [*Heimann et al.*, 1998]. *Trettin et al.* [2001] evaluated 12 popular soil C models and found that they did not adequately account for anoxia, alternating hydroperiods, complex interactions of soil chemistry and abiotic factors, CH_4 processes, and time steps that should be important to wetland C cycling.

[4] Existing wetland-related models generally fall into three categories: long-term peat accumulation models, empirical CH_4 emission models, and process-based CH_4 emission models. The peat accumulation models developed by *Clymo* [1984], *Frolking et al.* [2001], and others have been reviewed by *Yu et al.* [2001]. *Frolking et al.* [2001] developed a peat decomposition model (PDM) to calculate long-term peat accumulation based on vegetation conditions (NPP and rooting) and decomposition dynamics. This type of model focuses on long-term (several centuries to several millennia) peatland development and peat accumulation, and the effects of water table, vegetation, and climate are parameterized based on average conditions, usually for specific sites. Empirical CH_4 emission models have been developed by directly correlating the observed CH_4 fluxes to controlling factors, such as water table, soil temperature, plant primary productivity, or ecosystem productivity [e.g., *Bellisario et al.*, 1999; *Frolking and Crill*, 1994; *Moore and Roulet*, 1993; *Whiting and Chanton*, 1993; *Crill et al.*, 1988]. These empirical relationships cannot be extrapolated to other sites where conditions are different from the experimental sites. Process-based models simulate CH_4 emissions with different degrees of complexity and integration with other processes [*Cao et al.*, 1996; *Christensen et al.*, 1996; *Potter*, 1997; *Arah and Stephen*, 1998; *Grant*, 1998; *Walter and Heimann*, 2000; *Li*, 2000]. *Christensen et al.* [1996] estimated CH_4 emissions as a constant ratio of soil heterotrophic respiration under steady state conditions. *Potter* [1997] simulated CH_4 production (CH_4/CO_2 ratio) and CH_4 oxidation (fraction of CH_4) as functions of water table depth. *Walter and Heimann* [2000] and *Arah and Stephen* [1998] predicted CH_4 production and oxidation based on Michaelis-Menten kinetics and simulated CH_4 transportation in soil and via plants. Their maximum CH_4 production and oxidation rates were parameterized without integration with vegetation and soil decomposition processes, and the models need water table as input. *Cao et al.* [1996] considered the effects of environmental factors and substrates and the integrated processes of water table level, soil, and vegetation C dynamics in their simulation of CH_4 production and oxidation, although they used the Terrestrial Ecosystem Model (TEM) [*Raich et al.*, 1991] developed for upland ecosystems to handle the vegetation and soil C dynamics in their wetland studies. *Grant* [1998] simulated CH_4 emissions based on stoichiometries and energetics of the transformations mediated by each microbial community. His model may be the most complex CH_4 emission model, but was developed mainly for agricultural ecosystems. *Li* [2000] modified the DNDC model with detailed algorithms for simulating soil redox potential, substrate concentrations and CH_4 production, consumption and transport but only for rice paddies. We have adopted several of the above-listed approaches in the development of Wetland-DNDC, a more comprehensive wetland model.

[5] The purpose of developing Wetland-DNDC is to predict both CO_2 and CH_4 emissions driven by hydrology, soil biogeochemistry, and vegetation processes in wetland ecosystems. The model can run from a year to several decades with a primary time step of 1 day. This temporal scale allows us to directly use field observations to validate the model, and to answer questions about climatic change and management practices. The general structure of the model was adopted from PnET-N-DNDC, a process-oriented model simulating C and N dynamic and trace gas emissions in upland forest ecosystems [*Li et al.*, 2000]. PnET-N-DNDC was developed based on a basic biogeochemical concept, biogeochemical fields, which integrates the ecological drivers, environmental factors and geochemical and biochemical reactions into a dynamic system [*Li et al.*, 2000]. In comparison with the other 11 published biogeochemical models, PnET-N-DNDC provides a better framework for our development of a wetland C model [*Trettin et al.*, 2001]. For example, the ecological level and degree of complexity simulated by PnET-N-DNDC is a good match to the kinetic approaches adopted by *Walter and Heimann* [2000] and *Cao et al.* [1995, 1996] for modeling CH_4 fluxes from wetlands. In this paper, our discussion focuses on the new features developed in Wetland-DNDC, although Wetland-DNDC has inherited many existing functions from the DNDC model family (e.g., Crop-DNDC and PnET-N-DNDC). The distinguishing features of Wetland-DNDC include simulations of water table dynamics, effects of soil properties and hydrologic conditions on soil temperature, C fixation by mosses and herbaceous plants, and effects of anaerobic conditions on decomposition, CH_4 production and consumption, and other biogeochemical processes. The model validation tests against observations at three wetland sites in the U.S. and Canada are also reported here.

2. Model Description

[6] Wetland-DNDC consists of four components: hydrological conditions, soil temperature, plant growth, and soil C dynamics (Figure 1). These four components and their processes interact closely with each other. For example,

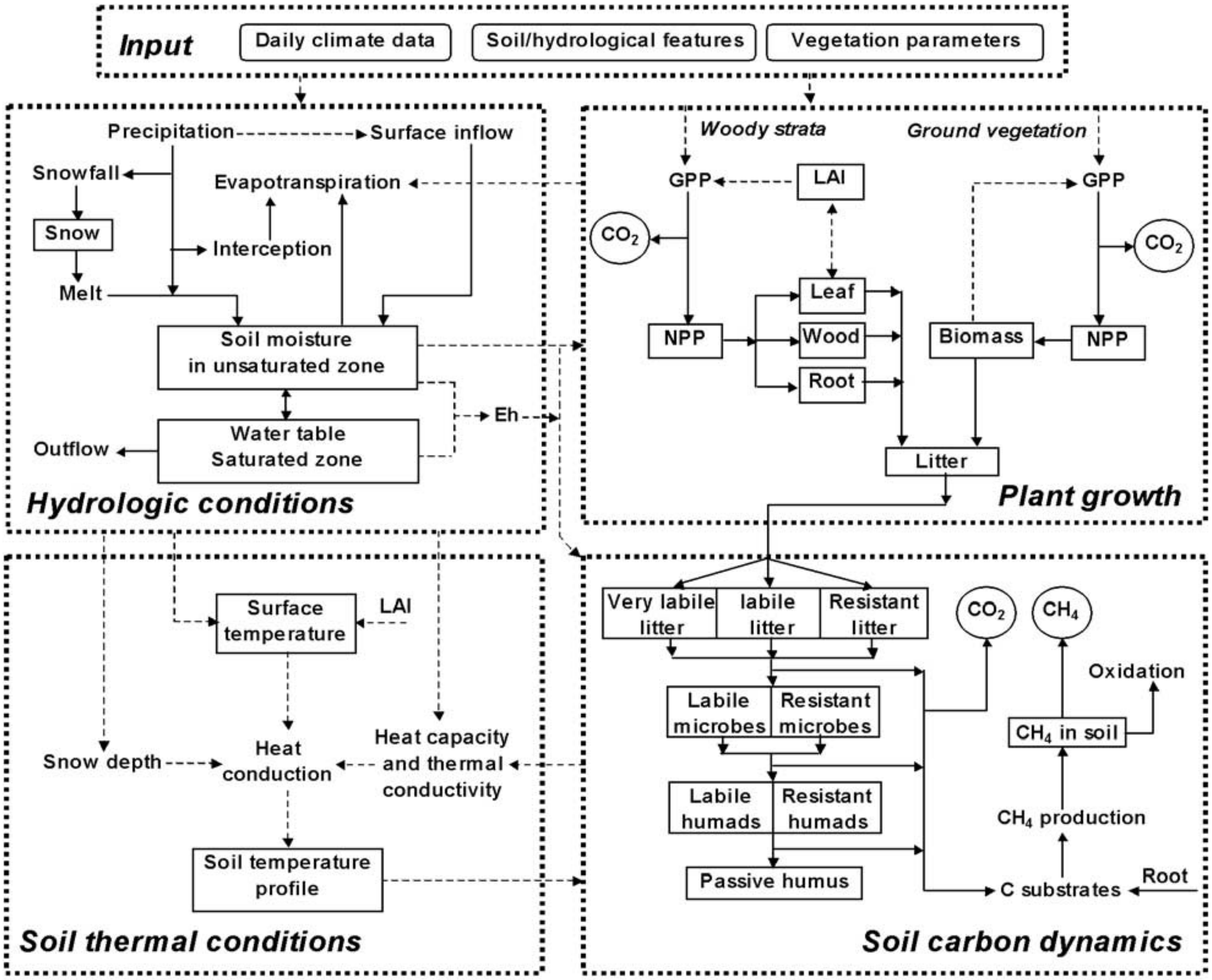

Figure 1. The conceptual structure of Wetland-DNDC. The model has four interacting components: hydrologic and thermal conditions, plant growth, and soil carbon dynamics. Solid lines are for matter flows, and dashed lines are information flows. Rectangles are for major state variables, and circles are for gas emissions.

soil thermal and hydrological conditions influence plant growth and soil C dynamics (e.g., decomposition, CH_4 production, and oxidation). Plant growth influences evapotranspiration and canopy interception and, thus, hydrological processes. Plant growth also affects CH_4 emissions by providing C substrates for CH_4 production and by providing conduits for CH_4 transport. Wetland-DNDC explicitly considers all these processes and their interactions (Figure 1). The state variables are expressed as mass per unit area or relative content, representing a spatially homogeneous area or site as defined by the input data. The model input includes initial conditions (e.g., plant biomass, soil porosity, soil C content, water table position), model parameters (e.g., lateral inflow/outflow parameters, maximum photosynthesis rate, respiration rate), and climate drivers (e.g., daily maximum and minimum temperature, precipitation, solar radiation). The model output includes C pools and fluxes (e.g., C in plants and soil, photosynthesis, plant respiration, soil decomposition, CH_4 emissions, and net ecosystem productivity), and thermal/hydrological conditions (e.g., soil moisture, water table position, water fluxes, soil temperature profile). Soil C pools and their decomposition processes are described in detail in DNDC [*Li et al.*, 1992], and the dynamics of woody stratum are described in PnET [*Aber et al.*, 1996; *Aber and Federer*, 1992]. Below we describe the major improvements and the new developments of Wetland-DNDC in (1) hydrology, (2) soil thermal dynamics, (3) growth of mosses and herbaceous plants, and (4) anaerobic processes (decomposition, CH_4 emissions).

2.1. Hydrology

[7] The hydrological submodel was developed to simulate water table dynamics explicitly. The soil profile is divided into layers of different characteristics (e.g., organic soils, mineral soils, and mineral soils with peat layers). The soil layers are then grouped into two zones: the unsaturated zone above the water table and the saturated zone below it. The

hydrological submodel considers water table dynamics, aboveground water input (e.g., precipitation, surface inflow, snow/ice melt) and output (evaporation, transpiration), and water movement in the unsaturated zone.

2.1.1. Soil Moisture and Water Table Dynamics

[8] The soil moisture content is determined for the unsaturated and the saturated zones separately. In the unsaturated zone, the soil moisture is determined by

$$\Delta \mathrm{SW}_l \cdot H_l = F_l - \mathrm{ES}_l - \mathrm{TP}_l \quad (1)$$

where $\Delta\mathrm{SW}_l$ is the change of soil moisture ($\mathrm{cm}^3 \cdot \mathrm{cm}^{-3}$) in layer l in the unsaturated zone, H_l is the thickness (cm) of the layer, F_l is net water input to the layer (cm water) through infiltration, gravity drainage, and matric redistribution, and ES_l and TP_l are water uptake (cm) from this layer through evaporation and transpiration, respectively. In the top saturated layer where water table resides (i.e., layer l_0), the soil moisture is estimated by

$$\mathrm{SW}_{l_0} = \mathrm{FC}_{l_0} + (\mathrm{PS}_{l_0} - \mathrm{FC}_{l_0})\mathrm{WT}'/H_{l_0} \quad (2)$$

where SW_{l_0} is the soil moisture ($\mathrm{cm}^3 \cdot \mathrm{cm}^{-3}$) of layer l_0, PS_{l_0} is the porosity ($\mathrm{cm}^3 \cdot \mathrm{cm}^{-3}$), FC_{l_0} is the field capacity ($\mathrm{cm}^3 \cdot \mathrm{cm}^{-3}$), WT' is the water table position in layer l_0 (cm above the bottom of layer l_0), and H_{l_0} is the thickness (cm) of the layer.

[9] Water table dynamics are determined directly by the water budget of the saturated zone, which includes water input from the unsaturated zone through infiltration and gravity drainage, capillary uptake through matric redistribution, evaporation and transpiration uptake from this zone, and outflow. The water budget is given by

$$\Delta \mathrm{WT}\,\mathrm{Yield} = F_{l_0} - \sum_{l=l_0}^{n} (\mathrm{ES}_l + \mathrm{TP}_l) - \mathrm{Outflow} \quad (3)$$

where $\Delta\mathrm{WT}$ is the change of water table position (cm), F_{l_0} is net water input (cm water) to the saturated zone from the above layers, and n is the total number of soil layers in the saturated zone. ES_l and TP_l are the same as those in equation (1). Yield ($\mathrm{cm}^3 \cdot \mathrm{cm}^{-3}$) and outflow (cm water) are defined as

$$\mathrm{Yield} = \begin{cases} \mathrm{PS}_{l_0} - \mathrm{SW}_{l_0} (\Delta \mathrm{WT} \geq 0) \\ \mathrm{PS}_{l_0} - \mathrm{FC}_{l_0} (\Delta \mathrm{WT} < 0) \end{cases} \quad (4)$$

$$\mathrm{Outflow} = \begin{cases} a_1(\mathrm{WT} - D_1) + a_2(\mathrm{WT} - D_2) & (\mathrm{WT} > D_1) \\ a_2(\mathrm{WT} - D_2) & (D_2 < \mathrm{WT} \leq D_1) \\ 0 & (\mathrm{WT} \leq D_2) \end{cases} \quad (5)$$

where $\mathrm{SW}_{l_0}, \mathrm{PS}_{l_0}$, and F_{l_0} are the same as those in equation (2), and WT is the water table position (cm) in reference to the soil surface. WT is positive when the water table is above the soil surface, and negative otherwise. $\Delta\mathrm{WT} > 0$ means that WT becomes higher. a_1, a_2, D_1, and D_2 are calibrated parameters for outflows. D_1 and D_2 represent two critical levels (cm) of WT. Outflow increases linearly when WT is higher than these levels. a_1 and a_2 are the rates of increase. Because D_1 is usually close to the surface and D_2 is deeper along the soil profile, $a_1(\mathrm{WT}\text{-}D_1)$ and $a_2(\mathrm{WT}\text{-}D_2)$ are regarded as surface outflow and ground outflow, respectively.

2.1.2. Aboveground Water Input and Output

[10] Aboveground water input includes precipitation, snow/ice melt, and surface inflow. We followed the work of *Running and Coughlan* [1988] to determine plant interception of precipitation and snowmelt

$$P_{\mathrm{int}} = \min(P, 0.05\,\mathrm{LAI}) \quad (6)$$

$$W_{\mathrm{melt}} = \min(\mathrm{SNOW}, 0.07 T_{\mathrm{m}}) \quad (T_{\mathrm{m}} > 0) \quad (7)$$

where P_{int} is the daily plant interception (cm), P is the daily precipitation (cm), and LAI is the leaf area index. W_{melt} is the amount of snow or ice melted in 1 day (cm in water), SNOW is the snowpack accumulated above the surface (cm in water), and T_{m} is the daily mean air temperature (°C). For depressional wetlands and most peatlands, surface lateral inflow usually comes from surface runoff of the watershed [*Mitsch and Gosselink*, 1993], and can be expressed as

$$S_{\mathrm{in}} = (r - 1) R_{\mathrm{p}} P \quad (8)$$

where S_{in} is the daily surface inflow (cm) expressed as water depth in the wetland, r is the ratio of the area of the watershed to the area of the wetland, and R_{p} is a hydrologic response coefficient. R_{p} represents the fraction of precipitation in the watershed that contributes directly to surface runoff. In the model, we combined $(r - 1)R_{\mathrm{p}}$ as one parameter (α_0).

[11] Both the potential evapotranspiration rate and water availability are considered in simulating evaporation and transpiration. We used the Priestley-Taylor approach [*Priestley and Taylor*, 1972; *Ritchie et al.*, 1988] to estimate potential evapotranspiration because it requires only daily solar radiation and temperature as input climate data. Potential evapotranspiration ($\mathrm{ET_p}$) is separated into potential soil evaporation ($\mathrm{ES_p}$) and potential plant transpiration ($\mathrm{TP_p}$) [*Ritchie et al.*, 1988]

$$\mathrm{ES_p} = \begin{cases} \mathrm{ET}_p(1 - 0.40\,\mathrm{LAI}) & (\mathrm{LAI} < 1) \\ \mathrm{ET}_p \exp(-0.43\,\mathrm{LAI}) & (\mathrm{LAI} \geq 1) \end{cases} \quad (9)$$

$$\mathrm{TP_p} = \mathrm{ET_p} - \mathrm{ES_p} \quad (10)$$

where $\mathrm{ES_p}$ and $\mathrm{TP_p}$ are in units of $\mathrm{cm \cdot day^{-1}}$. Evapotranspiration will first consume water intercepted by plants or water on the soil surface, and then water from the soil profile. The actual transpiration from a soil layer is determined by the potential demand and the root uptake rate

$$\mathrm{TP}_l = R_{\max} \mathrm{RLD}_l f_{\mathrm{ET},l} H_l \quad (11)$$

where TP_l is the water uptake rate from layer l ($\mathrm{cm\ water \cdot day^{-1}}$), $R_{\max}$ is the maximum water uptake rate of a unit root length density from a cubic centimeter soil ($\mathrm{cm\ water \cdot day^{-1} \cdot cm^{-1}\ root \cdot cm^{-3}\ soil}$), RLD_l is the root length density in layer l ($\mathrm{cm\ root \cdot cm^{-3}\ soil}$), H_l is the thickness (cm) of layer l, and $f_{\mathrm{ET},l}$ is a scalar. RLD_l is converted from root biomass using a specific root length of 2.1 $\mathrm{cm \cdot mg^{-1}}$ [*Eissenstat and Rees*, 1994]. $f_{\mathrm{ET},l}$ ranges from 0 to 1, representing the effects of soil moisture on evaporation and transpiration

$$f_{\mathrm{ET},l} = \begin{cases} 0 & (T_l < 0 \text{ or } \mathrm{SW}_l < \mathrm{WP}_l) \\ (\mathrm{SW}_l - \mathrm{WP}_l)/(\mathrm{FC}_l - \mathrm{WP}_l) & (\mathrm{WP}_l \leq \mathrm{SW}_l < \mathrm{FC}_l) \\ 1 & (\mathrm{SW}_l \geq \mathrm{FC}_l) \end{cases} \quad (12)$$

where WP_l is the soil moisture ($cm^3 \cdot cm^{-3}$) of layer l at the wilting point, FC_l is the field capacity ($cm^3 \cdot cm^{-3}$), and T_l is the soil temperature of layer l.

2.1.3. Water Movement in the Unsaturated Zone

[12] The hydrological submodel considers three types of water movement in the unsaturated zone: infiltration, gravity drainage, and matric redistribution. Daily infiltration is a function of the infiltration capacity and the amount of water available on the soil surface. If water available for infiltration is more than the infiltration capacity, the excessive water will stay on the surface as ponds. The infiltration capacity depends further on water table position, saturated conductivity, and the frozen layer depth. If no frozen layer exists and the water table is low, the infiltration capacity is estimated as the amount of water infiltrated in a period of 24 h. Otherwise, the infiltration capacity is the amount of water saturating all the layers above the frozen layer or above the water table level. Gravity drainage refers to the downward movement of water when soil moisture is higher than field capacity. In our model, we assume that a fraction of water above field capacity will move to the next layer each day. Matric redistribution refers to the water movement driven by the gradient of matric potential between layers. The movement can be upward or downward. Matric redistribution is estimated based on the soil moisture difference of the two adjacent layers [*Ritchie et al.*, 1988]. This procedure can include the capillary uptake of water from water table.

2.2. Soil Thermal Dynamics

[13] The soil temperature submodel estimates the daily average temperature of each soil layer by numerically solving the one-dimensional (vertical) heat conduction equation

$$C\frac{\partial T}{\partial t} = \frac{\partial}{\partial Z}\left(\lambda\frac{\partial T}{\partial Z}\right) \tag{13}$$

where C is the heat capacity ($J \cdot cm^{-3} \cdot {}^\circ C^{-1}$), T is the soil temperature (°C), t is time (s), λ is the thermal conductivity ($W \cdot cm^{-1} \cdot {}^\circ C^{-1}$), and Z is the soil depth (cm). The effects of soil water conditions and organic matter content on temperature can be expressed as their effects on C and λ

$$C = \sum_{i=1}^{5} f_i C_i \tag{14}$$

$$\lambda = \sum_{i=1}^{5} f_i \lambda_i \tag{15}$$

where f_i is the fraction (volumetric ratio) of a given soil component i (i.e., minerals, water, ice, organic matter, and air), and C_i and λ_i are the heat capacity and the thermal conductivity of component i, respectively.

[14] The temperature of the top and the bottom soil layers defines the boundary conditions needed to solve equation (13). The top layer can be snowpack (when a snowpack exists), or water (when there is no snowpack and the water table is above the surface), or soil (when a snowpack does not exist and the water table is below the surface). The temperature of the top layer is estimated based on the daily air temperature [*Zheng et al.*, 1993]

$$T_0 = \begin{cases} T_0' + 0.25(T_m - T_0')\exp(-K\mathrm{LAI}) & (T_m \geq T_0') \\ T_0' + 0.25(T_m - T_0') & (T_m < T_0') \end{cases} \tag{16}$$

where T_0 and T_0' are the temperatures of the top layer on the current day and the previous day, respectively, T_m is the air temperature on the current day, LAI is the leaf area index, and K is the light extinction coefficient. When a snowpack exists, mosses and herbaceous plants beneath the snowpack can effectively insulate heat conduction. Such insulation effects are considered by assuming a 5 cm moss/herbaceous layer with bulk density of 33.3 ($kg\ m^{-3}$) and water content of 0.4 ($g\ water \cdot g^{-1}$ biomass) [*Frolking et al.*, 1996]. The depth of the snowpack is estimated based on snow accumulation (snowfall and snowmelt) and snow density. We assume that precipitation will be in the form of snow when daily air temperature (T_m) is below 0°C. Snowpack is considered as one layer. Snow density increases each day by $0.001T_m$ when T_m is higher than 0°C, based on an approximation of a detailed hourly snow model [*Kongoli and Bland*, 2000]. Snow density is set to 0.1 $g \cdot cm^{-3}$ for fresh snow, and limited to 0.3 $g \cdot cm^{-3}$ as the upper value [*Verseghy*, 1991]. Snowmelt is a function of temperature [*Running and Coughlan*, 1988] (equation (7)). Thermal conductivity and heat capacity of snow are estimated based on snow density [*Mellor*, 1977].

[15] The bottom boundary temperature is estimated by

$$T_{Z_0} = T_{aa} + \exp(-Z_0/D)T_{am}\cos[2\pi(\mathrm{JD} - \mathrm{JD}_0)/365 - Z_0/D] \tag{17}$$

where T_{Z_0} is the soil temperature of the bottom layer with a depth of Z_0 (cm) on day JD, T_{aa} and T_{am} are the annual average and amplitude of air temperature, respectively, JD is the Julian date, and JD_0 is the Julian day when solar altitude is the highest (i.e., 200th and 20th for the Northern and the Southern hemispheres, respectively). D is the damping depth (cm), given by

$$D = [365 \times 864\lambda_m/(\pi C_m)]^{0.5} \tag{18}$$

where C_m is the average heat capacity of the soil profile ($J \cdot cm^{-3} \cdot {}^\circ C^{-1}$), and λ_m is the average thermal conductivity ($W \cdot cm^{-1} \cdot {}^\circ C^{-1}$) of the soil profile.

2.3. Growth of Mosses and Herbaceous Plants

[16] Mosses and herbaceous plants (hereafter, ground vegetation) are much more important for C fixation in wetlands compared to upland forest ecosystems. Therefore, we added algorithms for C fixation by ground vegetation to the vegetation submodel. Photosynthesis is estimated similarly to the moss simulation model of SPAM [*Frolking et al.*, 1996]

$$\mathrm{GPP_g} = A_{\max,g} B_g f_{g,L} f_{g,T} f_{g,W} \mathrm{DL} \tag{19}$$

where GPP_g is the daily gross photosynthesis of ground vegetation ($kg\ C \cdot ha^{-1} \cdot day^{-1}$), $A_{max,g}$ is the maximum photosynthesis rate per unit of effective photosynthetic biomass per hour ($kg\ C \cdot kg^{-1}\ C \cdot h^{-1}$), B_g is the effective

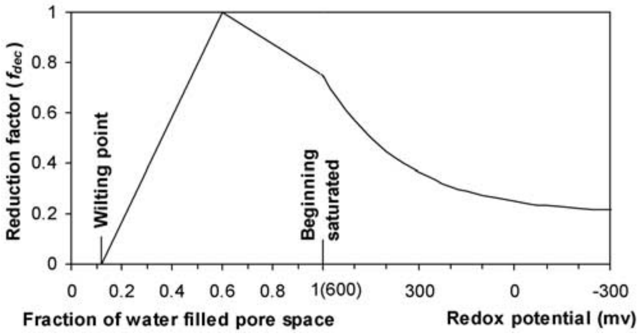

Figure 2. The effects of soil moisture (under unsaturated conditions) and redox potential (under saturated conditions) on soil organic carbon decomposition.

photosynthetic biomass of ground vegetation (kg C·ha^{-1}), DL is the day-length (hr·day^{-1}), and $f_{g,L}$, $f_{g,T}$, and $f_{g,W}$ are scalars that quantify the effects of light, temperature, and soil moisture, respectively. B_g is a function of the maximum aboveground biomass and the growing degree-days of the site; B_g represents changes in the amount of photosynthetically active tissues and the photosynthesis capacity of ground vegetation with time or phenology [*Skre and Oechel*, 1981; *Williams and Flanagan*, 1998]. We assume that the total daily respiration of plants is proportional to the daily GPP_g. Annual litter fall of ground vegetation is estimated as its annual net primary productivity (NPP) [*Frolking et al.*, 1996]. The growth of woody strata is simulated based on PnET [*Aber et al.*, 1996; *Aber and Federer*, 1992].

2.4. Anaerobic Processes

[17] In wetland ecosystems, soil C pools and fluxes and decomposition processes are strongly controlled by anaerobic conditions and, thus, hydrology. Anaerobic processes, such as CH_4 production and oxidation, are unique features of wet soils and are critical to our understanding and prediction of C dynamics in wetlands. To deal with soil anaerobic conditions, existing models use water table either to define the boundary between the anoxic and the oxic zones [*Walter and Heiman*, 2000], or to modify CH_4 production and oxidation rates [*Cao et al.*, 1996; *Potter*, 1997]. However, after the soil has been inundated, soil anaerobic status changes with time, and CH_4 production has a time delay of about 10 days [*Patrick and Reddy*, 1977]. In contrast, redox potential is a direct indicator of soil anaerobic status, and is closely related to the soil biochemical reactions [*Mitsch and Gosselink*, 1993; *Fiedler and Sommer*, 2000]. In Wetland-DNDC, we used the redox potential of the soil layers in the saturated zone to simulate the anaerobic effects on decomposition and CH_4 production and oxidation.

2.4.1. Redox Potential and SOC Decomposition

[18] Redox potential (*Eh*) is used to quantify the relative degree of anaerobic status for the soil layers near and below water table. *Eh* is estimated based on its general variation patterns in soils with a fluctuating water table [*Sigren et al.*, 1997] and in soils under continuously submerged conditions [*Patrick and Reddy*, 1977; *Fiedler and Sommer*, 2000]

$$\Delta Eh_l = \begin{cases} \mathrm{CR}(A_l - 1) & (l < l_0) \\ \mathrm{CR}(A_l + 1 - \mathrm{wfps}_l) & (l \geq l_0) \end{cases} \tag{20}$$

where ΔEh_l is the daily variation of redox potential of layer l (mv·day^{-1}), CR is the rate of change (i.e., 100 mv·day^{-1}), A_l is the aerenchyma factor of the layer, and wfps$_l$ is the fraction of water filled pore space when the water table is below the top of this layer. A_l defines the plant-mediated gas transport (i.e., equivalent to the fraction of pore space for gas diffusion).

$$A_l = \mathrm{FRD} P_A \mathrm{RLD}_l \tag{21}$$

where FRD is the area of the cross section of a typical fine root (cm^2), P_A is a scalar for the degree of gas diffusion from root to the atmosphere, and RLD$_l$ is the root length density (cm root·cm^{-3} soil) in layer l. FRD is assumed to be a constant of 0.0013 (cm^2) [*Barber and Silberbush*, 1984]. P_A ranges from 0 (plants without aerenchyma) to 1 (plants with well developed aerenchyma). Grasses and sedges are good gas transporters (P_A = 1), whereas trees are poor ones (P_A = 0.5). Mosses are not considered for this effect because they are not vascular plants (P_A = 0).

[19] Decomposition is slow under anaerobic conditions. The reported ratios of anaerobic decomposition to aerobic decomposition are 1:1.5–1:3 [*Bridgham and Richardson*, 1992], 1:2–1:4 [*Chamie and Richardson*, 1978], 1:3 [*DeBusk and Reddy*, 1998], 1:5 [*Clymo*, 1965], and 1:2.5–1:6 [*Moore and Dalva*, 1997]. Based on these results, we used the following relationship to estimate the effects of anaerobic status on decomposition for soil layers below the water table

$$f_{\mathrm{dec}} = 0.2 + 0.05 \exp\left(Eh/250\right) \tag{22}$$

where f_{dec} is a scalar for the anaerobic effects on decomposition. For the soil layers above water table, soil moisture is used to estimate f_{dec} [*Li et al.*, 1992]. Figure 2 shows the change of f_{dec} with changes of soil moisture and redox potential.

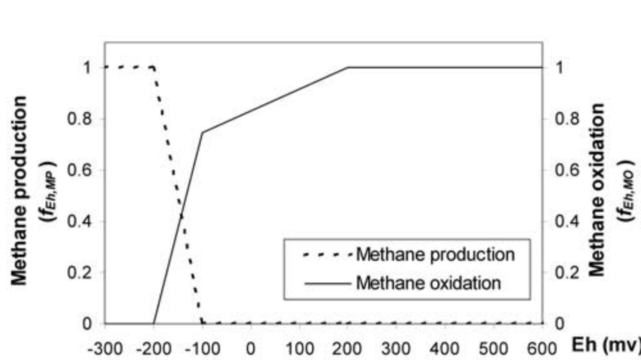

Figure 3. Effects of redox potential (*Eh*) on methane production ($f_{Eh,\ \mathrm{MP}}$) and oxidation ($f_{Eh,\ \mathrm{OX}}$). The relationships are generalized from the study of *Fieldler and Sommer* [2000], *Segers* [1998], and *Mitsch and Gosselink* [1993].

Table 1. The Initial Conditions, Model Parameters, and Data Sources at SSA-Fen

Parameters	Values	References
Lateral water flow		
Surface inflow (α_0)	0.2	calibrated[a]
Surface outflow (α_1, D_1)	0.0, 0	calibrated[a]
Ground outflow (α_2, D_2)	0.0002, −50	calibrated[a]
Ground vegetation		
Biomass, kg C·ha^{-1}	1950	*Suyker et al.* [1997]
$A_{\max,g}$, g C·kg^{-1} C·ha^{-1}	3.73	*Suyker et al.* [1997]
Respiration (fraction of daily GPP)	0.5	calibrated[a]
Half saturation light, μmol·m^{-2}·s^{-1}	40	*Frolking et al.* [1996]
Minimum, optimum and maximum GDD (°C·d)	500, 1200, 2300	calibrated[a]
Soil pH	7.1	*Suyker et al.* [1996]

[a] Lateral water flow parameters were calibrated by comparing the simulated and measured water table. Plant respiration parameter was determined by comparing the simulated and the measured annual NPP. Minimum, optimum and maximum growing degree days (GDD) were determined based on the phenology of the plant growth (beginning, maximum, and senescence) and climate data.

2.4.2. Methane Production, Oxidation, and Emissions

[20] To simulate CH_4 production, oxidation, and transport in Wetland-DNDC, we linked a process-based CH_4 emission model [*Walter and Heiman*, 2000] directly to soil thermal and hydrological conditions, soil redox potential, decomposition, and vegetation dynamics. Following the study by *Walter and Heiman* [2000], the change of CH_4 content in each layer (ΔM) is given by

$$\Delta M = M_{\mathrm{PRD}} - M_{\mathrm{OXD}} - M_{\mathrm{DFS}} - M_{\mathrm{EBL}} - M_{\mathrm{PLT}} \quad (23)$$

where M_{PRD} and M_{OXD} are the CH_4 production rate and the oxidation rate, respectively, M_{DFS} is the diffusion between layers or to the atmosphere, and M_{EBL} and M_{PLT} are the CH_4 emissions through ebullition and plant-mediated transport from the layer, respectively. All these terms are in unit of kg C·ha^{-1}·day^{-1}.

[21] Methane production occurs in all soil layers if there are enough substrates and if environmental conditions are favorable [*Fieldler and Sommer*, 2000]. We simulated CH_4 production from each layer, using an approach similar to the ones used by *Cao et al.* [1995, 1996] and *Walter and Heiman* [2000], but with explicit consideration of the effects of redox potential

$$M_{\mathrm{PRD}} = C_{\mathrm{M}} f_{\mathrm{T,MP}} f_{\mathrm{pH}} f_{Eh,\mathrm{MP}} \quad (24)$$

where C_M is the amount of simple C substrates (from soil decomposition and root systems) available for CH_4 production, and f_{pH}, $f_{\mathrm{T,MP}}$, $f_{Eh,\mathrm{MP}}$ are scalars for the effects of temperature, pH, and redox potential on CH_4 production, respectively. The C substrate from roots is estimated as 45% of the C transferred to roots from photosynthesis [*Cao et al.*, 1995]. We calculated the pH effect based on the study of *Cao et al.* [1995], but used a minimum pH of 4.0 (instead of 5.5) because CH_4 emissions have been observed when pH is below 5.5 in wetlands [*Crill et al.*, 1988; *Valentine et al.*, 1994]. *Walter and Heimann* [2000] use a Q_{10} value of 6 to represent the effects of temperature on CH_4 production. We used a Q_{10} value of 3 because the temperature effects on C_M for methanogenesis have already been included in the calculation for soil organic carbon decomposition [*Li et al.*, 1992]. Methanogenesis requires a very low redox potential. Based on measurements and the literature review by *Fiedler and Sommer* [2000], we used −200 and −100 mv as the two critical *Eh* values that define the effects of redox potential on CH_4 production (Figure 3).

[22] Methane oxidation is primarily controlled by the CH_4 concentration, redox potential, and temperature [*Segers*, 1998]. Methane oxidized in a soil layer is estimated by

$$M_{\mathrm{OXD}} = M f_{\mathrm{M}} f_{\mathrm{T,MO}} f_{Eh,\mathrm{MO}} \quad (25)$$

where M is the amount of CH_4 in a soil layer (kg C·ha^{-1}), and f_{M}, $f_{\mathrm{T,MO}}$, and $f_{Eh,\mathrm{MO}}$ are scalars, representing the effects of CH_4 concentration, temperature, and redox potential, respectively. Based on the work of *Walter and Heiman* [2000], the effects of CH_4 concentration are expressed as

$$f_{\mathrm{M}} = M_{\mathrm{C}}/(K_{\mathrm{m}} + M_{\mathrm{C}}) \quad (26)$$

where M_c is the CH_4 concentration in a layer (μmol·L^{-1}), and K_m is a constant (e.g., 5 μmol·L^{-1}) [*Walter and Heiman*, 2000]. A Q_{10} value of 2 is chosen to quantify the effects of soil temperature on the oxidation rate [*Segers*, 1998]. We consider the effects of redox potential on CH_4 oxidation (Figure 3) based on the general patterns of CH_4 oxidation rates and soil redox potentials [*Segers*, 1998; *Fiedler and Sommer*, 2000; *Mitsch and Gosselink*, 1993].

[23] The CH_4 diffusion process is estimated with empirical relationships. In a daily time step, the CH_4 concentration gradient between two adjacent layers in the saturated zone decreases by about 70%, and is fully mixed in air filled space. Actual diffusion rates between layers and from the top layer to the atmosphere were estimated based on soil water content.

[24] Methane in each layer can be directly emitted to the atmosphere through ebullition and plant−mediated emission [*Walter and Heiman*, 2000]. Ebullition emission is considered when the soil CH_4 concentration in a layer exceeded a threshold concentration of 750 μmol·L^{-1} [*Walter and Heiman*, 2000]. The plant-mediated emission is estimated based on the plant aerenchyma factor (i.e., A_l defined in equation (21))

$$M_{\mathrm{PLT}} = \mathrm{M}A_l(1 - P_{\mathrm{OX}}) \quad (27)$$

where M_{PLT} is plant-mediated emission from a soil layer (l), and P_{ox} is the fraction of CH_4 oxidized during the

Table 2. The Initial Conditions, Model Parameters, and Data Sources at MEF-Bog

Parameters	Values	References
Lateral water flow:		
Surface inflow (α_0)	0.5	calibrated[a]
Surface outflow (α_1, D_1)	0.05, 0	calibrated[a]
Ground outflow (α_2, D_2)	0.0005, −150	calibrated[a]
Ground vegetation		
Biomass, kg C·ha^{-1}	1750	*Grigal* [1985]
$A_{max,g}$, g C·kg^{-1} C·h^{-1}	1.57	*Skre and Oechel* [1981]
Respiration (fraction of daily GPP)	0.2	calibrated[a]
Half saturation light, μmol·m^{-2}·s^{-1}	40	*Frolking et al.* [1996]
Minimum, optimum and maximum GDD, °C·d	100, 1300, 2500	calibrated[a]
Soil pH	3.9	*Dise* [1991]
Woody stratum:		
Summer time LAI	1.74	*Grigal et al.* [1985]
Aboveground woody biomass, kg C·ha^{-1}	50365	*Grigal et al.* [1985]
Specific leaf area weight, g·m^{-2} leaf	180.7	*Gower et al.* [1997]
Root, kg C·ha^{-1}	71.3	*Grigal et al.* [1985] and *Gower et al.* [1997]
Foliage N concentration, %	0.88	*Gower et al.* [1997]
$A_{max,w}$, nmol CO_2·g^{-1}·s^{-1}	24.2	*Aber et al.* [1996]
Half saturation light, μmol·m^{-2}·s^{-1}	200	*Aber et al.* [1996]
Foliage retention time, yrs	11	*Gower et al.* [1997]
Begin and end foliage flushing GDD, °C·d	400, 1000	based on phenology and climate data
Begin senescence (Julian date)	230	based on phenology and climate data

[a] See the note in Table 1.

plant-mediated transport (i.e., 0.5) [*Walter and Heimann*, 2000].

3. Model Testing

[25] We tested Wetland-DNDC against field observations, including water table dynamics, soil temperature, CH_4 emissions, NEP, and annual C budget. A sensitivity analysis was also performed to determine critical parameters.

3.1. Sites and Data

[26] We selected three northern wetland sites where extensive measurements are available: one in Saskatchewan, Canada, and two in Minnesota, USA. The first wetland site is a minerotrophic fen located about 115 km northeast of Alberta, Saskatchewan, Canada (53°57′N, 105°57′W). This site (referred hereafter as SSA-Fen) is in the southern study area of the Boreal Ecosystem-Atmosphere Study (BOREAS) [*Sellers et al.*, 1997]. *Suyker et al.* [1996, 1997] give detailed descriptions of the site. Fluxes of CO_2 and CH_4 were measured in the growing seasons (from mid May to early October) of 1994 and 1995 by the eddy covariance technique, together with measurements of water table positions, plant species composition, and LAI [*Suyker et al.*, 1996, 1997]. All the data were obtained from the BOREAS CD-ROM [*Newcomer et al.*, 1999]. The second wetland site is a forested bog located in the Marcell Experimental Forest in Itasca County, Minnesota, USA (47°32′N, 93°28′W). This site (referred hereafter as MEF-Bog) is managed by the USDA Forest Service North Central Research Station. *Dise* [1991] and *Verry and Urban* [1992] give detailed descriptions of the site. *Dise* [1991] measured CH_4 emissions at MEF-Bog from 1989 to 1990 using open-bottom chambers, together with soil temperature and water table positions. In addition, the daily water table dynamics have been monitored since 1961 [*Verry and Urban*, 1991]. The third wetland site is a bog lake peatland located about 2 km from the MEF-Bog site. This site (referred hereafter as BLP-Fen) is characterized as a poor fen with carpet-forming mosses (*Sphagnum papillosum*) dominating the vegetation. Detailed descriptions of the site can be found in the study by *Shurpali et al.* [1993, 1995] and *Kim and Verma* [1992]. Both CO_2 and CH_4 fluxes were measured in 1991 and 1992 by the eddy covariance technique [*Shurpali et al.*, 1993, 1995].

3.2. Initial Conditions and Model Parameters

[27] The initial conditions and parameter values used in the model testing are given in Table 1 (SSA-Fen), Table 2 (MEF-Bog), and Table 3 (BLP-Fen). First, simulations were conducted based on different vegetation covers at the three sites. For SSA-Fen, the ground vegetation alone was used to determine the overall plant C fixation (Table 1) because of low tree density [*Suyker et al.*, 1997]. For MEF-Bog, both woody plants and ground vegetation were simulated explic-

Table 3. The Initial Conditions, Model Parameters, and Data Sources at BLP-Fen

Parameters	Values	References
Lateral water flow:		
Surface inflow (α_0)	1.0	calibrated[a]
Surface outflow (α_1, D_1)	0.1, 10	calibrated[a]
Ground outflow (α_2, D_2)	0.006, −50	calibrated[a]
Ground vegetation: parameters and their values are the same as those at MEF-Bog in Table 2		
Soil pH	4.6	*Kim and Verma* [1992]

[a] See the note in Table 1.

Table 4. The Soil Characteristics Along Soil Profiles Used in Simulations at the Three Study Sites[a]

Depth, cm	Bulk Density	Porosity	Field Capacity	Wilting Point
5	0.09	0.94	0.51	0.12
75	0.13	0.91	0.64	0.16
200	0.24	0.84	0.69	0.22

[a] The data are based on the works of *Zoitai et al* [2000] and *Paavilainen and Paivanen* [1995]. All of the four soil characteristics are in the unit $cm^3 \cdot cm^{-3}$.

itly (Table 2). For BLP-Fen, the same ground vegetation as for MEF-Bog was used, but woody plants were absent at this site (Table 3). Second, the active soil profile at the three sites was assumed to be 2 m in-depth and composed of peat. The distributions of bulk density, field capacity, and wilting point are given in Table 4, on the basis of the study by *Zoltai et al.* [2000] and *Paavilainen and Paivanen* [1995]. Third, the parameters of lateral water flow were determined by comparing the simulated and the measured water table (i.e., using the first 3 years' measurements at MEF-Bog and the 2 years' measurements at the other sites). Fourth, the micro-topographic effects (i.e., hollows and hummocks) on the overall C fluxes measured by the eddy covariance technique can be assessed based on the relative height of the peat surface [*Clement et al.*, 1995]. At MEF-Bog, the data for the microsites of hollows and hummocks were reported separately; thus, we ran the model for each micro site directly using the measured water table as input. At SSA-Fen and BLP-Fen, however, the micro-topographic effects were not reported. To better reflect these effects on C flux predictions, we obtained the average water table for the average hollow site, ran the model with this average water table and with four different surface heights above the hollow surface (i.e., 0, 10, 20, and 30 cm), calculated the average C fluxes from these four runs, and used the average C fluxes to compare with the tower measured C fluxes.

[28] Sensitivity analysis was conducted with the data from BLP-Fen in 1992 (Tables 3 and 4) as the baseline conditions. The model parameters, initial conditions, and climate drivers were changed one at a time to determine their effects on model predictions. The response variables used in the sensitivity analysis are water table, NPP, soil microbial respiration, CH_4 emissions, and NEP.

3.3. Results and Discussions

3.3.1. Hydrology

[29] The long-term measurements of water table dynamics from 1961 to 1999 at MEF-Bog provide an excellent data set for model validation. The model predictions correspond well to the trends and the temporal variations of the water table measurements (Figure 4). Comparisons between the simulated and the observed water table dynamics show good agreement (R^2 = 0.54, N = 14244); most of the unexplained variance may be a result of mismatches in the exact timing and exact values of water table change. The model also captured the variation patterns of surface outflow (Figure 5; R^2 = 0.52, N = 468), but the simulated surface outflow was about 46% higher than the measured stream outflow, perhaps due to water loss from places other than the measuring station at the stream outlet. The model estimates a ground outflow of 2–2.7 $cm \cdot month^{-1}$ (aside from a low value of 1.3 $cm \cdot month^{-1}$ in 1977). Although there was no direct measurement of ground outflow, a slow, steady seepage must have existed because the water table

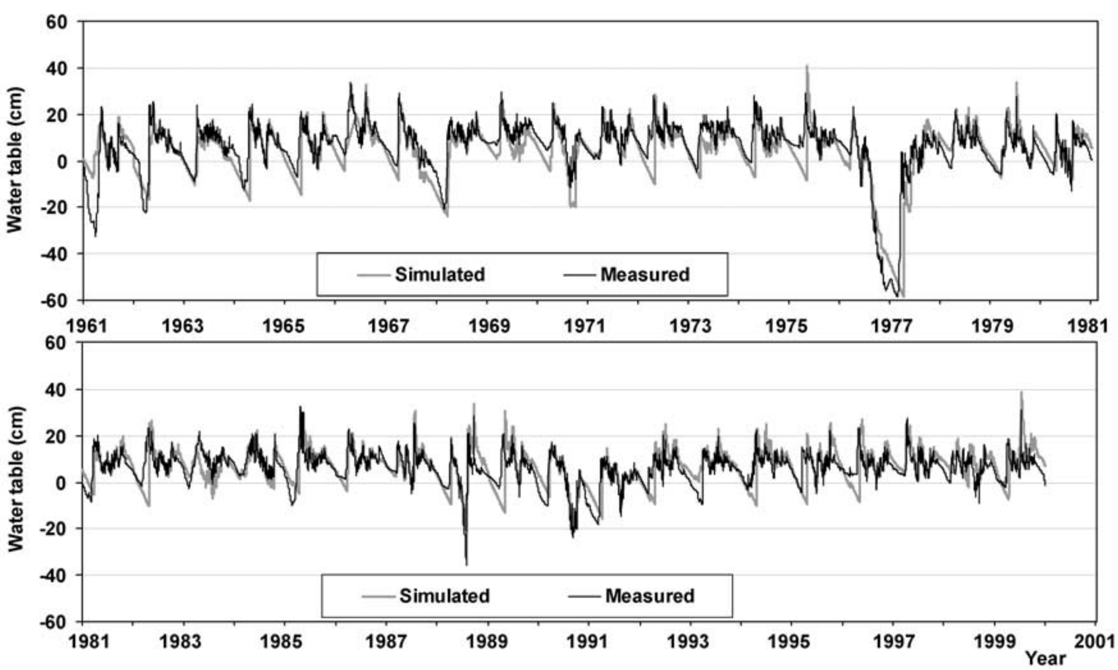

Figure 4. Comparisons between simulated and measured water table dynamics at MEF-Bog in Minnesota, USA.

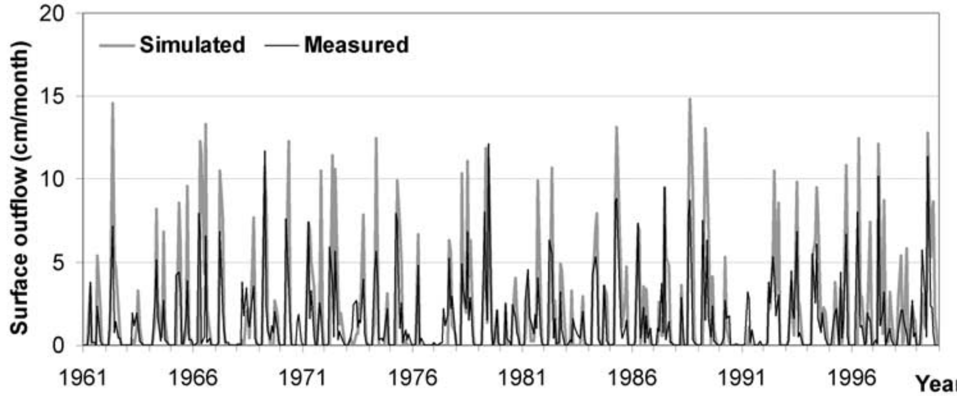

Figure 5. Comparisons between simulated and measured surface outflow at MEF-Bog in Minnesota, USA. The measurements were conducted at a stream outlet.

was perched several meters above the regional water table [*Verry and Urban*, 1992]. The model also works well in predicting evapotranspiration (R^2 = 0.62, N = 263. Years 1994 and 1996) and snowpack (R^2 = 0.83, N = 1021. Years 1994–1996) at SSA-Fen where measurements were available. These results indicate that the hydrologic model can successfully simulate water table dynamics and water fluxes of wetlands at the watershed scale.

3.3.2. Soil Temperature

[30] Soil temperature is an important factor in regulating soil decomposition and CH_4 emissions. Figure 6 shows comparisons between simulated and measured soil temperature at different depths of the hollow site at MEF-Bog. The model accurately predicts the trajectories of the measured soil temperature along the soil profile, with R^2 values ranging from 0.88 to 0.91 (with sample sizes of 45–59). Similar results are also obtained for the hummock site at MEF-Bog and for SSA-Fen (results not shown here). The model captures the effects of snow and soil organic matter on soil temperature. For example, due to the insulating effects of the moss layer and snowpack, soil temperature stays near or above 0°C in winter and spring although air temperature could be as low as −30°C. Soil temperature in deeper layers (e.g., 40 cm) may be 4°C lower than in the top layer in summer, but about 1°C higher in winter.

3.3.3. Methane Emissions

[31] The CH_4 emission model was tested at all three sites. The model captures general patterns of CH_4 emissions, including the annual total, inter-annual differences, and the effects of water table positions (Figure 7). Values of R^2 ranged from 0.37 to 0.76 with sample sizes of 47–214, except at MEF-Bog hummock, where R^2 = 0.03 (N = 42), because CH_4 emission is very low. At SSA-Fen, CH_4 emissions are largely correlated with plant growth and soil decomposition because the water table is almost always above the surface. The simulated annual CH_4 emissions (kg C·ha^{-1}·yr^{-1}) are 122.1 for 1994 and 121.0 for 1995 (Figure 7A). The estimated CH_4 emissions from the tower flux measurements were 163 kg C·ha^{-1} for the period from May 17 of 1994 to October 7 of 1994 [*Suyker et al.*, 1996]. The difference between simulated and observed CH_4 emissions in 1994 may be caused by an underestimation of peak CH_4 emissions and late growing season emissions. Although the water table was above the hollow surface, it showed larger fluctuations in 1994 than in 1995. In 1994, the water table increased from 5 cm in late May to 26 cm in late July, then declined to 3 cm in late September. In 1995, the water table declined from 25 cm in late May to 14 cm in late September. In general, the model overestimates CH_4 emissions when water table increases, but underestimates CH_4 emissions when water table decreases. We suspect that these simulation errors may be caused by: (1) combination effects of micro-topography and water table fluctuation, (2) trapping and releasing of CH_4 during water table fluctuations, and (3) effects of water layer thickness since the model assumes that the water table will have the same effects on anaerobic

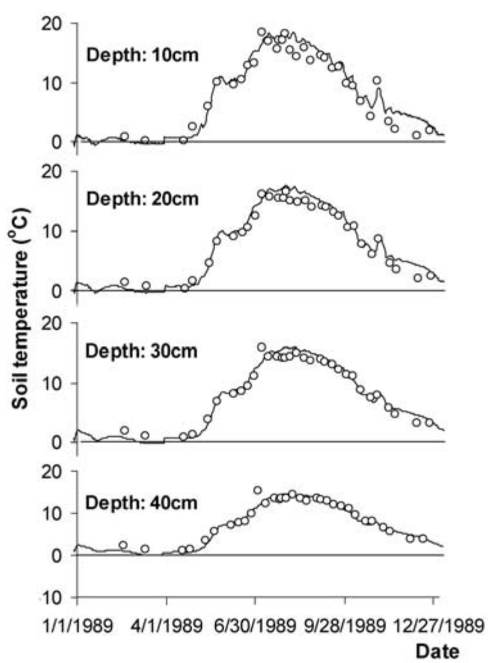

Figure 6. Comparisons between simulated (curves) and measured (dots) soil temperature along a soil profile at MEF-Bog in Minnesota, USA. The data are for the hollow site measured by *Dise* [1991].

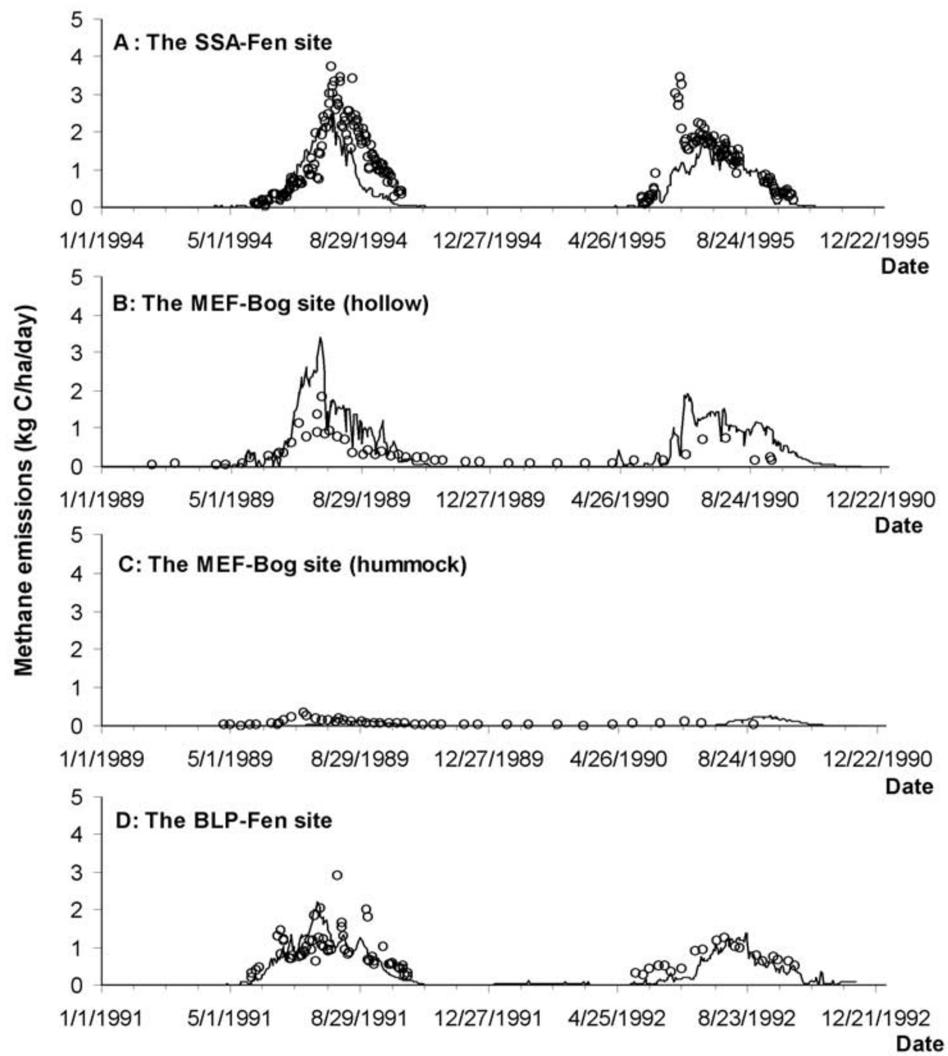

Figure 7. Comparisons between simulated (curves) and measured (dots) methane emissions at the three study sites: SSA-Fen in Saskatchewan, Canada, MEF-Bog (hollow versus hummock) in Minnesota, USA, and BLP-Fen in Minnesota, USA. The measurements at BLP-Fen in 1991 are daytime totals from the work of *Shurpali et al.* [1993], while all other measurements and the simulated results are daily totals.

conditions and CH_4 transport when water table is above the surface, regardless of depth.

[32] At MEF-Bog, CH_4 emissions from the hummock site are much smaller than those from the hollow site (Figure 7B, C) because the average water table for the hummocks is 38 cm below the surface compared to 7 cm below the surface for the hollows. The simulated annual CH_4 emissions (kg $C \cdot ha^{-1} \cdot yr^{-1}$) for the hollow site are 157.1 for 1989 and 127.0 for 1990, while they are 8.6 for 1989 and 14.0 for 1990 at the hummock site. The estimated CH_4 emissions (kg $C \cdot ha^{-1}$) from observations from April 1 of 1989 to March 31 of 1990 were 103.5 for the hollows and 26.3 for the hummocks [*Dise*, 1991].

[33] At BLP-Fen, the model predictions display good agreement with the observations (Figure 7D). Note that in Figure 7D, the CH_4 measurements of 1991 are the daytime totals reported by *Shurpali et al.* [1993], whereas the measurements for 1992 are daily totals reported by *Clement et al.* [1995]. The simulated annual CH_4 emissions are 129.2 kg $C \cdot ha^{-1} \cdot yr^{-1}$ for 1991, which is within the range of the observed values of 120.0–146.3 kg $C \cdot ha^{-1} \cdot yr^{-1}$ reported for 1991 [*Shurpali et al.*, 1993]. The simulated annual CH_4 emissions for 1992 are 87.8 kg $C \cdot ha^{-1} \cdot yr^{-1}$. The lower CH_4 value in 1992 may be due to the relatively stable and high water table that limits soil decomposition and, therefore, reduces C substrates for CH_4 production.

3.3.4. CO_2 Flux and C Budget

[34] Wetland-DNDC also predicts other C fluxes and the annual C budget in addition to CH_4 emissions. Figure 8 shows the variation patterns of NEP, NPP, and soil decomposition (i.e., soil microbial CO_2 emissions) at SSA-Fen and BLP-Fen. There were no observed daily fluxes of NPP and soil decomposition at these two sites. However, we present the simulated NPP and soil decomposition to aid in understanding the variation patterns of NEP and the annual C budget.

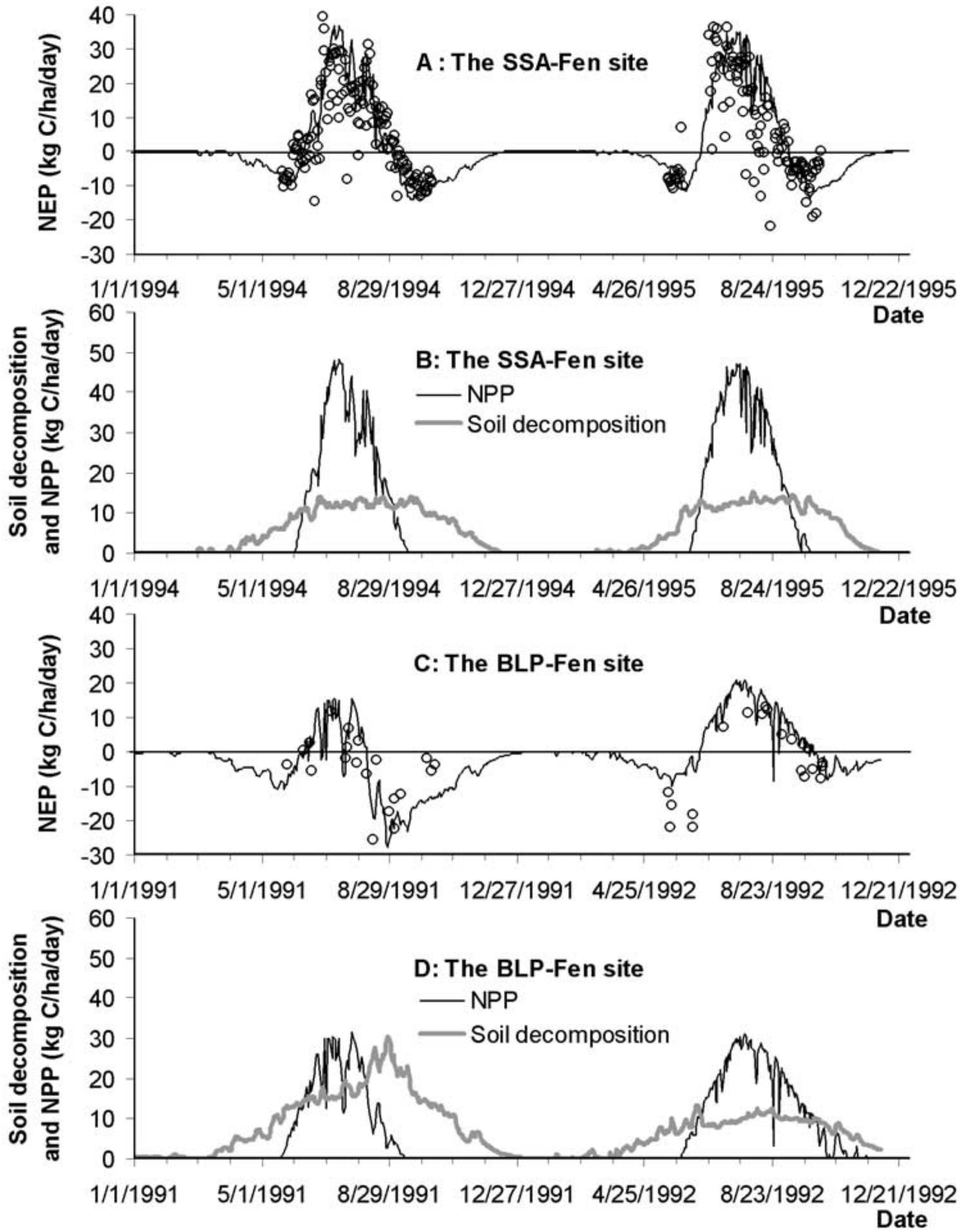

Figure 8. The temporal dynamics of net ecosystem exchange (NEP), net primary productivity (NPP), and soil decomposition. (a) Comparisons between simulated and measured NEP at SSA-Fen; (b) simulated NPP and soil decomposition at SSA-Fen; (c) comparisons between simulated and measured NEP at BLP-Fen; and (d) simulated NPP and soil decomposition at BLP-Fen.

[35] At SSA-Fen, predicted NEP was compared to the measured daily NEP during the period of 1994–1995. The model captures the general pattern of NEP (Figure 8A) (R^2 = 0.49, N = 266). The simulated total NEP from mid–May to early October in 1994 is 958.4 kg C$\cdot$ha^{-1}, which agrees closely with the measured NEP of 880 kg C$\cdot$ha^{-1} for the same period [*Suyker et al.*, 1997]. NEP is a function of the combined effects of plant C fixation and soil C decomposition (Figure 8B). The simulated annual NPP (kg C$\cdot$ha$^{-1}\cdot$yr^{-1}) is 2589.8 for 1994 and 2878.1 for 1995, while the field measured aboveground NPP in 1994 was 1950 kg C$\cdot$ha$^{-1}\cdot$yr^{-1} [*Suyker et al.*, 1996]. The simulated soil decomposition (kg C$\cdot$ha$^{-1}\cdot$yr^{-1}) is 2128.3 for 1994 and 2023.9 for 1995. The annual C sequestration (kg C$\cdot$ha$^{-1}\cdot$yr^{-1}), which included CO_2 exchange and CH_4 emissions, is calculated as 339.4 for 1994 and 733.2 for 1995. The average annual C sequestration for these 2 years is 536.3 kg C$\cdot$ha$^{-1}\cdot$yr^{-1}. This value is higher than the average long-term wetland C accumulation rate (210 kg C$\cdot$ha$^{-1}\cdot$yr^{-1}) estimated by *Clymo et al.* [1998], perhaps because this site is more productive than moss-dominated wetlands and because the high water table during these 2 years may have reduced soil decomposition.

Table 5. Simulated Annual Carbon Budget of the MEF-Fen Site[a]

Year		1989			1990		
		Woody Strata	Ground Vegetation	Total	Woody Strata	Ground Vegetation	Total
Hollow	GPP	7129.9	1986.5	9116.4	7538.8	2194.1	9732.9
	NPP	3647.8	1589.2	5237.0	3877.4	1755.3	5632.7
	plant growth	2318.7	0.0	2318.7	2496.7	0.0	2496.7
	litter production	1329.1	1589.2	2918.3	1380.7	1755.3	3136.0
	soil microbial respiration			1864.8			2495.8
	CH_4 emissions			157.1			127.0
	soil C balance			896.4			513.2
	C sequestration			3215.1			3009.9
Hummock	GPP	8589.7	1999.6	10589.3	7779.7	2196.5	9976.2
	NPP	3933.8	1599.7	5533.5	4026.2	1757.2	5783.4
	plant growth	2532.5	0.0	2532.5	2604.3	0.0	2604.3
	litter production	1401.3	1599.7	3001.0	1421.9	1757.2	3179.1
	soil microbial respiration			2954.3			3487.3
	CH_4 emissions			8.6			14.0
	soil C balance			38.1			−322.2
	C sequestration			2570.6			2282.1

[a]Unit: kg C ha^{-1} yr^{-1}.

[36] At BLP-Fen, the model also captures the general pattern of NEP, displaying good agreement between the predicted and the measured daily NEP during the period of 1991–1992 (Figure 8C) ($R^2 = 0.59$, $N = 40$). The simulated NEP (kg C·ha^{-1}) for the period from mid May to mid October is −910.2 for 1991 and 931.0 for 1992, while the measured NEP for the same period was −710 for 1991 and 320 for 1992 [*Shurpali et al.*, 1995]. The simulated NEP for early 1992 is much higher than the measurements largely because the model fails to capture the sizable C release during the pre-leaf period when C trapped in soils from decomposition in late fall and winter was released as soil thawed [*Lafleur et al.*, 1997]. The simulated NPP of the ground vegetation shows a rapid decline and then an early termination in the fall of 1991 (Figure 8D) because of drought effects. During the period of May–October, total precipitation in 1991 was about 30% less than that in 1992, and the mean temperature in 1991 was 1.5°C higher than that in 1992. The simulated annual NPP (kg C·ha^{-1}·yr^{-1}) is 1754.2 for 1991 and 2436.9 for 1992. The simulated soil decomposition rate also reflects drought effects (i.e., high temperature, low precipitation, low water table) in 1991; the peak soil decomposition rate in 1991 was twice that in 1992 (Figure 8D). The simulated soil decomposition for the period from May to October of 1991 is 2939.3 kg C·ha^{-1}, which is comparable to the measured value of 3654.5 kg C·ha^{-1} (including root respiration) [*Kim and Verma*, 1992]. The simulated annual NEP (kg C·ha^{-1}·yr^{-1}) is −1581.8 for 1991 (source) and 470.7 for 1992 (sink). The annual C sequestration (kg C·ha^{-1}·yr^{-1}), including CO_2 exchange and CH_4 emissions, is −1711.0 for 1991 and 382.9 for 1992.

[37] There is no woody stratum at SSA-Fen and BLP-Fen. The annual change in soil C therefore is the same as NEP because we assume that the annual NPP of ground vegetation should be the same as its litter production. Table 5 shows the simulated annual C budget at MEF-Bog. Both the hollow and hummock sites are sinks of atmospheric CO_2 with the C accumulation occurring primarily in the woody strata. Although the mortality of the trees may greatly reduce this sequestration, as measured by *Grigal et al.* [1985], the model currently does not consider mortality. Soil C increases at the hollow site, but changes little in 1998 and even decreases in 1990 at the hummock site. The average soil C balance of the hollow and hummock sites is 281.4 kg C·ha^{-1}·yr^{-1}, which is comparable to the 180–280 kg C·ha^{-1}·yr^{-1} estimated by *Verry and Urban* [1992]. They also found a soil C loss with water flow of 370 kg C·ha^{-1}·yr^{-1}. However, their estimate of soil microbial respiration (4710 kg C·ha^{-1}·yr^{-1}) was much higher than our simulated results. As a result, their estimate of litter input to soil would also be much higher, possibly due to tree mortality. The simulated NPP is 5434.9 and 5658.5 kg C·ha^{-1}·yr^{-1} at the hollow and hummock sites, respectively; these numbers are comparable to the above ground NPP of 3700 kg C·ha^{-1} ·yr^{-1} measured by *Grigal* [1985] and *Grigal et al.* [1985].

3.3.5. Sensitivity Analysis

[38] Sensitivity analysis reveals the effects of given factors on selected state variables. The three groups of factors are initial conditions, model parameters, and climate drivers, while the five selected state variables are water table (WT), NPP, soil microbial respiration (R_s), CH_4 emissions, and NEP. WT is given as absolute change, whereas the others are expressed as percent change (Table 6).

[39] The five state variables respond differently to different input variables. WT and NPP are sensitive to only a few model parameters and environmental variables, whereas R_s, CH_4, and NEP respond strongly to many (Table 6). One simple reason is that calculating C fluxes like CH_4 and NEP involves many components of Wetland-DNDC. WT is primarily influenced by hydrological parameters (e.g., the critical levels of outflow; D_1 and D_2 in (5)) and by climate variables (e.g., precipitation, temperature). A decrease in either D_1 or D_2 by 10 cm could lower the annual average

Table 6. Sensitivity Analysis of Wetland-DNDC[a]

Input Parameters and Variables	Change	ΔWT[b], cm	ΔNPP, %	ΔR_s, %	ΔCH_4, %	ΔNEP, %
		Initial Conditions				
Biomass	+10%	0.0	8.7	0.1	4.5	13.6
	−10%	0.0	−9.2	−0.1	−4.6	−14.6
Soil organic carbon	+10%	0.0	0.0	9.9	12.6	−12.5
	−10%	0.0	0.0	−9.9	−9.7	12.5
Soil pH	+0.5	0.0	0.0	0.0	18.3	0.0
	−0.5	0.0	0.0	0.0	−20.1	0.0
Porosity	+10%	0.0	−0.4	−5.0	−18.6	5.7
	−10%	−1.7	0.5	6.9	8.9	0.0
Field capacity	+10%	−1.3	0.0	−3.5	3.0	4.4
	−10%	0.0	0.0	−0.2	−3.6	0.2
		Parameters				
Surface inflow (α_0)	+10%	0.3	−0.1	−2.8	−3.7	3.5
	−10%	−1.5	0.2	0.7	−13.2	−0.6
Surface outflow rate (α_1)	+10%	−0.1	0.0	−0.3	−4.3	−0.4
	−10%	0.2	0.0	0.1	0.9	0.1
Ground outflow rate (α_2)	+10%	−2.5	0.2	−1.5	−14.1	2.2
	−10%	1.1	−0.1	−6.1	4.7	7.6
Critical level for surface outflow (D_1)	+10 cm	5.5	−0.1	−1.2	6.9	1.4
	−10 cm	−9.2	2.2	18.1	−51.4	−19.3
Critical level for ground outflow (D_2)	+10 cm	5.1	−0.1	−13.4	3.9	16.8
	−10 cm	−10.3	1.0	10.6	−28.8	−7.8
$A_{max,g}$	+10%	0.0	9.0	0.0	4.7	14.4
	−10%	0.0	−9.3	0.0	−4.8	−14.9
Half saturation light	+10%	0.0	−0.9	0.0	−0.4	−1.5
	−10%	0.0	0.9	0.0	0.4	1.5
Respiration rate	+10%	0.0	−2.3	0.0	−1.2	−3.7
	−10%	0.0	2.3	0.0	1.2	3.7
Minimum GDD	+100°C·d	0.0	−3.8	0.0	−1.7	−6.0
	−100°C·d	0.0	−3.9	0.0	1.6	6.1
Optimal GDD	+100°C·d	0.0	−0.3	0.0	−0.6	−0.5
	−100°C·d	0.0	0.6	0.0	0.5	0.9
Maximum GDD	+100°C·d	0.0	1.9	0.0	0.5	3.0
	−100°C·d	0.0	2.4	0.0	−0.6	3.8
Climate drivers[c]						0.0
Temperature	+2°C	−2.0	−12.4	63.5	10.5	−99.9
	−2°C	−2.1	−0.5	−35.6	−48.1	44.2
Precipitation	+10%	0.8	−0.1	−4.4	1.5	5.4
	−10%	−5.0	0.8	6.3	−20.9	−6.6
Solar radiation	+10%	−0.1	0.0	1.3	−0.4	0.0
	−10%	0.0	0.0	0.0	0.0	0.0

[a] The parameters are changed from the baseline data of BLP-Fen in Table 3, either by 10% or by a specified quantity. The selected response variables are the annual average water table (ΔWT), net primary production (ΔNPP), soil microbial respiration (ΔR_s), net ecosystem productivity (ΔNEP), and methane emissions (ΔCH4).
[b] Water table is expressed as the annual average, while the others are expressed as the annual totals.
[c] Changes of climate drivers are for each day based on daily climate data.

WT by about 10 cm (Table 6); this is because outflow increases linearly with WT as soon as WT rises above these boundary levels. Such high sensitivity of WT to D_1 and D_2 indicates that good long-term WT data are essential since D_1 and D_2 (together with a_1 and a_2,) are calibrated parameters (5). Furthermore, although an increase in precipitation may produce limited effects on WT, a drought may exert greater influences on WT (Table 6). NPP is sensitive to the maximum photosynthesis rate ($A_{max,g}$ in equation (18)) and the initial biomass, similar to what was observed by *Aber et al.* [1996] for woody plants. In addition, while NPP shows little response to a decrease in temperature, it may be reduced by 12.4% with a 2°C temperature increase, perhaps because of increasing autotrophic respiration. R_s is significantly affected by temperature because temperature exerts direct effects on microbial activity and on soil moisture conditions. The simulations show that the number of days when WT is above the surface decreases dramatically from 171 days under the baseline condition to 85 days with a temperature increase of 2°C. R_s is also sensitive to changes in D_1 and D_2 and initial soil organic C. CH_4 responds strongly to temperature and D_1 and D_2, and, to a lesser extent, to precipitation and initial soil conditions (e.g., organic C, pH, and porosity). For NEP, the most critical factors are temperature, D_1 and D_2, $A_{max,g}$, plant biomass, and initial soil organic C.

[40] To further test the interactions between plant, soil, and hydrology, we conducted two simulation experiments. First, we arbitrarily controlled the C substrates for CH_4 production. Simulated annual CH_4 emissions decrease 49.4% when C substrates from plants are eliminated, while simulated CH_4 emissions decrease 69.6% when C substrates from soil decomposition are excluded. Second, we ran the model with constant water table levels (i.e., 20, 10, and 0

cm above the surface, and 10, 20, and 30 cm below the surface). When the water table is maintained at 10 cm above surface, annual CH_4 emissions are the highest, 89% of the baseline emissions. When water table is kept at 20 cm above surface, annual CH_4 emissions decrease by about 30% compared to that observed for a water table 10 cm above the surface due to a decrease in soil decomposition and soil temperature. This suggests that a fluctuating water table may be more favorable for CH_4 emissions than a constant water table. Because the effect of water table on NPP is small, change in NEP is mostly due to the effect of water table on soil heterotrophic respiration. NEP is 1205.7 kg $C \cdot ha^{-1} \cdot yr^{-1}$ with a water table 20 cm above the surface and -706.8 kg $C \cdot ha^{-1} \cdot yr^{-1}$ with a water table 30 cm below the surface. The baseline NEP is 396.7 kg $C \cdot ha^{-1} \cdot yr^{-1}$. These results and those from sensitivity analysis show that C dynamics and CH_4 emissions respond differently to input factors and are quite sensitive to the processes and interactions between thermal/hydrological conditions, plant growth, and soil C dynamics. It is therefore critical for models to integrate hydrology, vegetation, soil, and climate in predicting C exchange and CH_4 emissions of wetland ecosystems.

4. Conclusions

[41] A biogeochemical model, Wetland-DNDC, was developed by integrating the complex processes of hydrology, soil biogeochemistry, and vegetative growth in wetland ecosystems. In comparison to its parent model (PnET-N-DNDC), Wetland-DNDC includes several important changes, which enable the new model to work well for the specific conditions found in wetlands. The major improvements include functions and algorithms for simulating water table dynamics, the effects of soil composition and hydrologic conditions on soil temperature, C fixation by mosses or other ground growth species, and the effects of anaerobic status on decomposition and CH_4 production/oxidation. Wetland-DNDC was tested against data sets of observed water table dynamics, soil temperature, CH_4 flux, CO_2 exchange, and annual C budget at three wetland sites in North America. The modeled results are in agreement with the observations at the three sites. Sensitivity analysis indicates that wetland C dynamics are sensitive to temperature, water outflow rate, initial soil organic C content, plant photosynthesis capacity, and initial biomass in the wetland ecosystems. NEP and CH_4 fluxes are sensitive to a wide scope of input parameters of climate, soil, hydrology, and vegetation. The ecosystem C dynamics as well as the CH_4 emissions simulated by Wetland-DNDC respond to changes in thermal and hydrological conditions in a complex manner. The results further confirm the necessity of utilizing process models for predicting C dynamics driven by the many interactions among climate, hydrology, soil, and vegetation in the wetland ecosystems.

[42] Wetland-DNDC currently does not include distribution hydrological routines to handle water inflow and outflow for a given watershed due to the complexity in calculation and amount of spatially differentiated input data required (e.g., topography, soil etc.). Instead, we focused this model at the site scale, and empirically parameterized the inflow and outflow indices for individual wetland watersheds where multiple-year observations of water table dynamics were available. For applying the model at large scales, these hydrological indices can be generated based on the normalized ranges or variations in water table and the lateral water fluxes. In this case, uncertainty analysis must be conducted to assess the potential errors produced from the generalized hydrological parameters.

[43] To overcome this limitation in the current version of Wetland-DNDC, we plan to develop a watershed-scale hydrological submodel to improve the model's performance.

Notation

A_l, plant aerenchyma factor of layer l.
A_0 plant specific aerenchyma factor, (cm^2).
$A_{\mathrm{max,g}}$ maximum photosynthesis rate of ground vegetation (kg $C \cdot kg\ C^{-1} \cdot h^{-1}$).
$A_{\mathrm{max,w}}$ maximum photosynthesis rate of woody plant (nmol $CO_2 \cdot g^{-1} \cdot s^{-1}$).
B_g efficient photosynthetic biomass of ground vegetation (kg $C \cdot ha^{-1}$).
C heat capacity of a layer ($J \cdot cm^{-3} \cdot {}^\circ C^{-1}$).
C_i heat capacity of component i ($J \cdot cm^{-3} \cdot {}^\circ C^{-1}$).
C_M C substrate for CH_4 production in a soil layer (kg $C \cdot ha^{-1}$).
CR change rate of soil redox potential under saturated conditions (100 $mv \cdot day^{-1}$).
D damping depth (cm).
D_1, D_2 critical depths for lateral outflow (cm).
D_l depth of soil layer i (cm).
DL day length ($hr \cdot day^{-1}$).
Eh redox potential (mv).
ES_l water lost through evaporation from layer l (cm).
ES_P potential soil evaporation (cm).
ET_P potential evapotranspiration (cm).
f_{dec} effects of redox potential and soil moisture on decomposition.
f_i volumetric fraction of component i in soil.
$f_{\mathrm{g,GDD}}$ effects of growing degree days on amount of effective photosynthetic biomass.
$f_{\mathrm{gL}}, f_{\mathrm{g,T}}, f_{\mathrm{g,W}}$ effects of light, temperature, and water on photosynthesis of ground vegetation, respectively.
$f_{\mathrm{ET},l}$ effects of soil moisture on evaporation and transpiration.
$f_{Eh,\mathrm{MP}}$ effects of redox potential on CH_4 production.
$f_{Eh,\mathrm{MO}}$ effects of redox potential on CH_4 oxidation.
f_M effects of CH_4 concentration on CH_4 oxidation.
F_{pH} effects of pH on CH_4 production.
$f_{T,\mathrm{MP}}$ effects of temperature on CH_4 production.
$f_{\mathrm{T,MO}}$ effects of temperature on CH_4 oxidation.
FC_{l_0} field capacity of soil layer l_0 ($cm^3 \cdot cm^{-3}$).
F_l, F_{l_0} net water input to layer l and l_0, respectively, through infiltration, gravity drainage, and matric redistribution (cm).

FRD the area of the cross-section of a typical fine root (0.0013 cm^2).
GPP_g gross photosynthesis of ground vegetation (kg C·ha^{-1}).
H_l, H_{l_0} thickness of layer l and l_0, respectively (cm).
JD Julian date.
JD_0 Julian date when solar altitude is the highest (200 for the Northern hemisphere, 20 for the Southern hemisphere).
K_m a constant (5 μmol·L^{-1}) for effects of CH_4 concentration on CH_4 oxidation (μ mol·L^{-1}).
l_0 soil layer in which water table resides.
LAI leaf area index (one side area) (m^2·m^{-2}).
M CH_4 content in a soil layer (kg C·ha^{-1}).
M_c CH_4 concentration in a layer (μ mol·L^{-1}).
M_{DIF} CH_4 content decrease through diffusion (kg C·ha^{-1}).
M_{EBL} CH_4 emission through ebullition (kg C·ha^{-1}).
M_{PLT} CH_4 emission through plant-mediated transport (kg C·ha^{-1}).
M_{OXD} CH_4 oxidation rate of a soil layer (kg C·ha^{-1}).
M_{PRD} CH_4 production in a soil layer (kg C·ha^{-1}).
N Sample size.
n number of layers above water table level.
Outflow lateral outflow from the saturated zone (cm).
P Precipitation (cm).
P_A relative capacity of a plant for gas diffusion from its root system to the atmosphere.
P_{int} plant interception of precipitation (cm).
P_{ox} fraction of CH_4 oxidized during plant mediated transport (0.5).
PS_{l_0} porosity of soil layer l_0 (cm^3·cm^{-3}).
R^2 squared correlation coefficient.
r ratio of the area of a watershed to the area of a wetland in the watershed.
RLD_l root length density of layer l (cm^{-2}).
R_{max} maximum root water uptake rate (0.003 cm^2·day^{-1}).
R_p the surface-runoff fraction of precipitation in a watershed.
S_{in} surface inflow (cm).
SNOW snowpack (cm water).
SW_l, SW_{l_0} soil moisture of layer l and l_0, respectively (cm^3·cm^{-3}).
t, time (s).
T, T_l soil temperature (°C).
T_0,T'_0 top surface temperature on the current day and the day before, respectively (°C).
T_{aa} annual average air temperature (°C).
T_{am} annual amplitude of air temperature (°C).
T_{Z_0} bottom layer soil temperature (°C).
T_m daily mean air temperature (°C).
TP_l water lost through transpiration from layer l (cm).
TP_P potential plant transpiration (cm).
$wfps_l$ fraction of water filled pore space.
W_{melt} snowmelt (cm water).
WP_l soil moisture at wilting point of layer l (cm^3·cm^{-3}).
WT water table position in reference to soil surface (cm).
WT′ height of water table level above the bottom of layer l_0 (cm).
Yield amount of water required for a unit water table change (cm cm^{-1}).
Z depth (cm).
Z_0 depth of the bottom soil layer (cm).
α_0 surface inflow relative to precipitation.
α_1,α_2 rate parameters for outflow.
λ thermal conductivity of a layer (W·cm^{-1}·°C^{-1}).
λ_I thermal conductivity of component i (W·cm^{-1} ·°C^{-1}).
ΔM change of CH_4 content in a soil layer (kg C·ha^{-1}·day^{-1}).
ΔEh change of redox potential (mv·day^{-1}).
ΔSW_l change of soil moisture in layer l in the unsaturated zone (cm^3·cm^{-3}·day^{-1}).
ΔWT change of water table position (cm·day^{-1}).

[44] **Acknowledgments.** The authors gratefully acknowledge the contributions of the source codes of PnET-N-DNDC provided by John Aber, Florien Stange, Klaus Butterback-Bahl, and Hans Papen. The authors are indebted to Nigel Roulet for supporting Yu Zhang to conduct his study in McGill University. The authors would like to thank the two anonymous reviewers for their comments and suggestions, and Karen Bartlett for editing the paper. This study is funded by the USDA Forest Service Southern Global Change Program, U.S. multiagency TECO grant, and NASA EOS-IDS grant.

References

Aber, J. D., and C. A. Federer, A generalized, lumped-parameter model of photosynthesis, evaporation and net primary production in temperate and boreal forest ecosystems, *Oecologia*, *92*, 463–474, 1992.
Aber, J. D., P. B. Reich, and M. L. Goulden, Extrapolating leaf CO_2 exchange to the canopy: A generalized model of forest photosynthesis compared with measurements by eddy correlation, *Oecologia*, *10*, 257–265, 1996.
Arah, J. R. M., and K. D. Stephen, A model of the processes leading to methane emission from peatland, *Atmos. Environ.*, *32*, 3257–3264, 1998.
Aselmann, I., and P. J. Crutzen, Global distribution of natural freshwater wetlands and rice paddies, their net primary productivity, seasonality and possible methane emissions, *J. Atmos. Chem.*, *8*, 307–358, 1989.
Barber, S. A., and M. Silberbush, Plant root morphology and nutrient uptake, in *Roots, Nutrient and Water Influx, and Plant Growth, American Society of Agronomy*, edited by S. A. Barber and D. R. Bouldin. *Spec. Publ. 49*, pp. 65–87, Madison, WI, 1984.
Bellisario, L. M., J. L. Bubier, T. R. Moore, and J. P. Chanton, Controls on CH_4 emissions from a northern peatland, *Global Biogeochem. Cycles*, *13*, 81–91, 1999.
Bridgham, S. D., and C. J. Richardson, Mechanisms controlling soil respiration (CO_2 and CH_4) in southern peatlands, *Soil Biol. Biochem.*, *24*, 1089–1099, 1992.
Bubier, J. L., The relationship of vegetation to methane emission and hydrochemical gradients in northern peatlands, *J. Ecol.*, *83*, 403–420, 1995.
Bubier, J. L., P. M. Crill, T. R. Moore, K. Savage, and R. K. Varner, Seasonal patterns of controls on net ecosystem CO_2 exchange in a boreal peatland complex, *Global Biogeochem. Cycles*, *12*, 703–714, 1998.
Cao, M., J. B. Dent, and O. W. Heal, Modeling methane emissions from rice paddies, *Global Biogeochem. Cycles*, *9*, 183–195, 1995.
Cao, M., S. Marshall, and K. Gregson, Global carbon exchange and methane emissions from natural wetlands: Application of a processes-based model, *J. Geophys. Res.*, *101*, 14,399–14,414, 1996.
Chamie, J. P. M., and C. J. Richardson. Decomposition in northern wetlands, in *Freshwater Wetlands: Ecological Processes and Management Potential*, edited by R. E. Good, D. F. Whigham, and R. L. Simpson. pp. 115–130, Academic, San Diego, Calif., 1978.

Christensen, T. R., I. C. Prentice, J. Kaplan, A. Haxeltine, and S. Sitch, Methane flux from northern wetlands and tundra: An ecosystem source modeling approach, *Tellus, Ser. B*, *48*, 652–661, 1996.

Clement, R. J., S. B. Verma, and E. S. Verry, Relating chamber measurements to eddy correlation measurements of methane flux, *J. Geophys. Res.*, *100*, 21,047–21,056, 1995.

Clymo, R. S., Experiments on breakdown of sphagnum in two bogs, *J. Ecol.*, *53*, 747–758, 1965.

Clymo, R. S., Limit of peat bog growth, *Philos. Trans. R. Soc. London, Ser. B*, *303*, 605–654, 1984.

Clymo, R. S., J. Turunen, and K. Tolonen, Carbon accumulation in peatland, *Oikos*, *81*, 368–388, 1998.

Crill, P. M., K. B. Bartlett, R. C. Harriss, E. Gorham, E. S. Verry, D. I. Sebacher, L. Madzar, and W. Sanner, Methane flux from Minnesota peatlands, *Global Biogeochem. Cycles*, *2*, 371–384, 1988.

DeBusk, W. F., and K. R. Reddy, Turnover of detrital organic carbon in a nutrient-impacted Everglades marsh, *Soil Sci. Soc. Am. J.*, *62*, 1460–1468, 1998.

Dise, N. B., Methane emission from peatlands in Northern Minnesota, Ph.D dissertation, p. 138, Univ. of Minnesota, Minneapolis, 1991.

Eissenstat, D. M., and K. C. J. Van Rees, The growth and function of pine roots, *Ecol. Bull.*, *43*, 76–91, 1994.

Eswaran, H., E. Van den Berg, P. Reich, and J. Kimble. Global soil carbon resources, in *Soils and Global Change*, edited by R. Lal et al., pp. 27–43, CRC Press, Boca Raton, Fla., 1995.

Fiedler, S., and M. Sommer, Methane emissions, ground water levels and redox potentials of common wetland soils in a temperate-humid climate, *Global Biogeochem. Cycles*, *14*, 1081–1093, 2000.

Frolking, S., and P. Crill, Climate controls on temporal variability of methane flux from a poor fen in southeastern New Hampshire: Measurement and modeling, *Global Biogeochem. Cycles*, *8*, 385–397, 1994.

Frolking, S., et al., Modelling temporal variability in the carbon balance of a spruce/moss boreal forest, *Global Change Biol.*, *2*, 343–366, 1996.

Frolking, S., N. T. Roulet, T. R. Moore, P. J. H. Richard, M. Lavoie, and S. D. Muller, Modeling northern peatland decomposition and peat accumulation, *Ecosystems*, *4*, 479–498, 2001.

Gorham, E., Northern peatlands: Role in the carbon cycle and probable response to climate warming, *Ecol. Monogr.*, *1*, 182–195, 1991.

Grant, R. F., Simulation of methanogenesis in the mathematical model ecosys, *Soil Biol. Biochem.*, *30*, 883–896, 1998.

Grigal, D. F., *Sphagnum* production in forested bogs of northern Minnesota, *Can. J. Bot.*, *63*, 1204–1207, 1985.

Grigal, D. F., C. G. Buttleman, and L. K. Kernik, Biomass and productivity of woody strata of forested bogs in northern Minnesota, *Can. J. Bot.*, *63*, 2416–2424, 1985.

Heimann, M., et al., Evaluation of terrestrial carbon cycle models through simulations of the seasonal cycle of atmospheric CO_2: First results of a model intercomparison study, *Global Biogeochem. Cycles*, *12*, 1–24, 1998.

Kim, J., and S. B. Verma, Soil surface CO_2 flux in a Minnesota peatland, *Biogeochemistry*, *18*, 37–51, 1992.

Kongoli, C. E., and W. L. Bland, Long-term snow depth simulation using a modified atmosphere-land model, *Agric. For. Meteorol.*, *104*, 273–287, 2000.

Lafleur, P. M., J. H. McCaughey, D. W. Joiner, P. A. Bartlett, and D. E. Jelinski, Seasonal trends in energy, water, and carbon dioxide fluxes at a northern boreal wetland, *J. Geophys. Res.*, *102*, 29,009–29,020, 1997.

Li, C., Modeling trace gas emissions from agricultural ecosystems, *Nutr. Cycling Agroecosyst.*, *58*, 259–276, 2000.

Li, C., S. Frolking, and T. A. Frolking, A model of nitrous oxide evolution from soil driven by rainfall events, 1, Model structure and sensitivity, *J. Geophys. Res.*, *97*, 9759–9776, 1992.

Li, C., J. Aber, F. Stange, and H. Papen, A process-oriented model of N_2O and NO emissions from forest soils, 1, Model development, *J. Geophys. Res.*, *105*, 4369–4384, 2000.

Matthews, E., and I. Fung, Methane emission from natural wetlands: Global distribution, area and environmental characteristics of sources, *Global Biogeochem. Cycles*, *1*, 61–86, 1987.

Mellor, M., Engineering properties of snow, *J. Glaciol.*, *19*, 15–66, 1977.

Mitsch, W. J., and J. G. Gosselink, *Wetlands*, 2nd ed., p. 722, Van Nostrand Reinhold, New York, 1993.

Mitsch, W. J., M. Sraskraba, and S. E. Jorgensen (Eds.), *Wetland Modeling: Development in Environmental Modeling*, vol. 12, p. 227, Elsevier Science, New York, 1988.

Moore, T. R., and M. Dalva, Methane and carbon dioxide exchange potentials of peat soils in aerobic and anaerobic laboratory incubations, *Soil Biol. Biochem.*, *29*, 1157–1164, 1997.

Moore, T. R., and N. T. Roulet, Methane flux: Water table relations in northern wetlands, *Geophys. Res. Lett.*, *20*, 587–690, 1993.

Newcomer, J., et al., (Eds), *Collected Data of the Boreal Ecosystem-Atmosphere Study*, (CD-ROM), NASA, 1999.

Paavilainen, E., and J. Päivänen, *Peatland Forestry, Ecology and Principles*, p. 248, Springer-Verlag, New York, 1995.

Patrick, W. H., Jr., and C. N. Reddy, Chemical changes in rice soils, in *IRRI Symposium on Soils and Rice*, pp. 361–379, IRRI, Los Bano., Philippines, 1977.

Potter, C. S., An ecosystem simulation model for methane production and emission from wetlands, *Global Biogeochem. Cycles*, *11*, 495–506, 1997.

Priestly, C. H. B., and R. J. Taylor, On the assessment of surface heat flux and evaporation using large scale parameters, *Mon. Weather Rev.*, *100*, 81–92, 1972.

Raich, J. W., E. B. Rastetter, J. M. Melillo, D. W. Kicklighter, P. A. Stendler, B. J. Peterson, A. L. Grace, B. Moore III, and C. J. Vorosmarty, Potential net primary productivity in South America: An application of a global model, *Ecol. Appl.*, *1*, 399–429, 1991.

Ritchie, J. T., D. C. Godwin, and S. Otter-Nache, *CERES-Wheat. A Simulation Model of Wheat Growth and Development*, Texas A&M Univ. Press., College Station, TX, 1988.

Running, S. W., and J. C. Coughlan, A general model of forest ecosystem processes for regional application, 1, Hydrologic balance, canopy gas exchange and primary production processes, *Ecol. Modell.*, *42*, 125–154, 1988.

Segers, R., Methane production and methane consumption: A review of processes underlying wetland methane fluxes, *Biogeochemistry*, *41*, 23–51, 1998.

Sellers, P. J., et al., BOREAS in 1997: Experiment overview, scientific results, and future directions, *J. Geophys. Res.*, *102*, 28,731–28,769, 1997.

Shurpali, N. J., S. B. Verma, R. J. Clement, and D. P. Billesbach, Seasonal distribution of methane flux in a Minnesota peatland measured by eddy correlation, *J. Geophys. Res.*, *98*, 20,649–20,655, 1993.

Shurpali, N. J., S. B. Verma, J. Kim, and T. J. Arkebauer, Carbon dioxide exchange in a peatland ecosystem, *J. Geophys. Res.*, *100*, 14,319–14,326, 1995.

Sigren, L. K., S. T. Lewis, F. M. Fisher, and R. L. Sass, Effects of field drainage on soil parameters related to methane production and emission from rice paddies, *Global Biogeochem. Cycles.*, *11*, 151–162, 1997.

Silvola, J., J. Alm, U. Ahlholm, H. Nykanen, and P. J. Martikainen, CO_2 fluxes from peat in boreal mires under varying temperature and moisture conditions, *J. Ecol.*, *84*, 219–228, 1996.

Skre, O., and W. C. Oechel, Moss functioning in different Taiga ecosystems in interior Alaska, *Oecologia*, *48*, 50–59, 1981.

Suyker, A. E., S. B. Verma, R. J. Clement, and D. P. Billesbach, Methane flux in a boreal fen: Season-long measurement by eddy correlation, *J. Geophys. Res.*, *101*, 28,637–28,647, 1996.

Suyker, A. E., S. B. Verma, and T. J. Arkebauer, Season-long measurement of carbon dioxide exchange in a boreal fen, *J. Geophys. Res.*, *102*, 29,021–29,028, 1997.

Trettin, C. C., B. Song, M. F. Jurgensen, and C. Li, *Existing Soil Carbon Models do not Apply to Forested Wetlands*, USDA Forest Service GTR SRS-46, 2001.

Valentine, D. W., E. A. Holland, and D. S. Schimel, Ecosystem and physical controls over methane production in northern wetlands, *J. Geophys. Res.*, *99*, 1563–1571, 1994.

Verry, E. S., and N. R. Urban, Nutrient cycing at Marcell Bog, Minnesota, *Suo*, *43*, 147–153, 1992.

Verseghy, D. L., CLASS - A Canadian land surface scheme for GCMs, I, Soil model, *Int. J. Climatol.*, *11*, 111–133, 1991.

Walter, B. P., and M. Heimann, A process-based, climate-sensitive model to derive methane emissions from natural wetlands: Application to five wetland sites, sensitivity to model parameters, and climate, *Global Biogeochem. Cycles*, *14*, 745–765, 2000.

Williams, T. G., and L. B. Flanagan, Measuring and modeling environmental influences on photosynthetic gas exchange in Sphagnum and Pleurozium, *Plant Cell Environ.*, *21*, 555–564, 1998.

Whiting, G. J., and J. P. Chanton, Primary production control of methane emission from wetlands, *Nature*, *364*, 794–795, 1993.

Yu, Z., I. D. Campbell, D. H. Vitt, and M. J. Apps, Modelling long-term peatland dynamics, I, Concepts, review, and proposed design, *Ecol. Modell.*, *145*, 197–210, 2001.

Zheng, D., E. R. Hunt Jr., and S. W. Running, A daily soil temperature model based on air temperature and precipitation for continental applications, *Clim. Res.*, *2*, 183–191, 1993.

Zoltai, S. C., R. M. Siltanen, and J. D. Johnson, *A Wetland Data Base for* *the Western Boreal, Subarctic, and Arctic Regions of Canada, Inform. Rep. NOR-X-368*, p. 30, Natural Resources Canada, Canada Forest Service, Northern Forestry Center, Edmonton, 2000.

C. Li, Complex Systems Research Center, Institute for the Study of Earth, Ocean and Space, University of New Hampshire, Durham, NH 03824, USA.

H. Li and C. C. Trettin, Center for Forested Wetlands Research, USDA Forest Service, 2730 Savannah Hwy., Charleston, SC 29414, USA. (lih@cofc.edu)

G. Sun, Southern Global Change Program, North Carolina State University, 920 Main Campus Dr. Venture II, Suite 300, Raleigh, NC 27606, USA.

Y. Zhang, Environmental Monitoring Section, Canada Center for Remote Sensing, 588 Booth Street, Ottawa, Ontario, Canada K1A 0Y7. (yu.zhang@ccrs.nrca.gc.ca)